Research in
Astronomy and
Astrophysics

Intra-day variability of three Seyfert galaxies measured with *XMM-Newton*

Ashutosh Tripathi[1], Paul Joseph Wiita[2,3], Alok Chandra Gupta[4,5], Min-Feng Gu[5] and Mai Liao[5,6]

[1] Center for Field Theory and Particle Physics and Department of Physics, Fudan University, Shanghai 200433, China; *ashutosh31tripathi@yahoo.com*

[2] Department of Physics, The College of New Jersey, P.O. Box 7718, Ewing, NJ 08628-0718, USA

[3] Kavli Institute for Particle Physics and Cosmology, SLAC, 2575 Sand Hill Rd., Menlo Park, CA, 94025, USA

[4] Aryabhatta Research Institute of Observational Sciences (ARIES), Manora Peak, Nainital - 263 002, India

[5] Key Laboratory for Research in Galaxies and Cosmology, Shanghai Astronomical Observatory, Chinese Academy of Sciences, Shanghai 200030, China

[6] University of Chinese Academy of Sciences, Beijing 100049, China

Abstract We present and analyze the variability of three Seyfert galaxies on intra-day timescales. We have analyzed in a uniform manner the 38 longest (> 30 ks) observations made for NGC 4051, MCG-06–30–15 and NGC 4151 by *XMM-Newton* between 2000 and 2015. The nuclei were quite active during essentially all of these observations and the overall X-ray fluxes (0.3–10 keV) varied by an order of magnitude. Most of the observations do appear to show characteristic timescales, estimated through their auto-correlation functions, ranging between $\sim$2.9 ks and $\sim$45.3 ks. The hard (2–10 keV) and soft (0.3–2.0 keV) bands are very well correlated but consideration of their hardness ratios shows that the sources typically soften during flares. We also provide new estimates of the central black hole masses for these three AGNs that support the hypothesis that Narrow Line Seyfert 1 galaxies have relatively small central black holes.

Key words: galaxies: active — narrow line Seyfert 1 galaxy (NLSy1): general — NLSy1: individual — NLSy1: individual: NGC 4051

1 INTRODUCTION

Narrow-line Seyfert 1 galaxies (NLSy1) share most general properties of Seyfert type 1 galaxies, including both narrow and broad emission lines and significant core flux variability, but their permitted emission lines have relatively small widths. The full width at half maximum of the Hβ lines in these galaxies are $\lesssim$2000 km s^{-1} (Goodrich 1989) with the ratio O[III]/Hβ $<$ 3 (Boller et al. 1996; Véron-Cetty et al. 2001). Their spectra show signatures of Fe II multiplets which anti-correlate with the O[III] emission and with the width of broad Balmer lines in their spectra. These characteristics support the conclusion that the broad line regions and the accretion disks around their central supermassive black holes (SMBHs) can be viewed without any blockage, as is the case in general for Seyfert type 1 galaxies (e.g. Komossa & Xu 2007). X-ray spectra of these galaxies show more variability than those of AGNs with broader emission lines. All of these proper-

ties are consistent with their being AGNs with relatively low SMBH masses and high accretion rates and thus high Eddington ratios. Characteristic timescales for variability in AGNs have been proposed to scale directly with the SMBH mass (e.g. Markowitz et al. 2003; Papadakis 2004). However, the NLSy1s do not neatly fit into this framework and this behavior could be explained by the dependence of timescales on another parameter, such as black hole spin or accretion rate (e.g. Ishibashi & Courvoisier 2009; Zhou et al. 2015; Pan et al. 2016).

The X-ray flux variations of AGNs on various timescales have, of course, been investigated frequently (e.g. Edelson & Nandra 1999; Gaur et al. 2010; González-Martín & Vaughan 2012; Kalita et al. 2015; Gupta et al. 2016; Pandey et al. 2017, and references therein). Most of the sources considered for those studies are Seyfert galaxies or blazars as they exhibit the most rapid fluctuations in their observed fluxes, but Seyferts have the advantage in that they are much closer and usually have

higher count rates, despite the Doppler boosting and temporal interval enhancements from which blazars benefit. Typical time-scales have been found to be less than a day, which is commonly known as intra-day variabilty (IDV) (Wagner & Witzel 1995). In the last decade, there have been some claims for the presence of quasi-periodic oscillations (QPOs) in AGN X-ray time series data on IDV timescales (e.g. Espaillat et al. 2008; Gierliński et al. 2008; Lachowicz et al. 2009; Pan et al. 2016; and references therein). Variabilities of AGNs on these IDV timescales are the most puzzling. The study of characteristic AGN timescales is important as they can give insight about the emission mechanisms and the innermost regions of AGNs. We, therefore, have started examining X-ray IDV in Seyfert galaxies. In the first paper of this project, we present here an analysis of X-ray IDV measured using *XMM-Newton* as exhibited by two NLSy1 galaxies, NGC 4051 and MCG–06–30–15, as well as that of NGC 4151, a Seyfert 1.5 galaxy.

Our aim in this paper is to search for and characterize IDV in Seyfert galaxies. We selected these sources because they have been examined for rapid X-ray variability in the past and have been shown to be active. For instance, Vaughan et al. (2011) analyzed 17 pointed observations of NGC 4051 taken during May 2001 to June 2009. They stacked the light curves of all observations together and then computed a single power spectral density (PSD); however, they did not analyze the individual light curves of NGC 4051 to examine them for IDV. For MCG-06–30–15, McHardy et al. (2005) performed a PSD analysis of the *RXTE* long-term light curve of MCG-06–30–15 that was observed between 1996 to 2004. They also included an analysis of some observations taken by *XMM-Newton*, producing a combined PSD analysis of 2–10 keV *RXTE* and 4–10 keV *XMM-Newton* light curves. In these earlier works, the galaxies were studied for the purpose of understanding the emission mechanisms and the accretion disk. Our studies, however, focus on searching for the variability of the order of a day, which means we only analyzed the observations longer than 30 ks. We are also concerned with any differences in the variability over soft and hard X-ray energy bands and so we also examined the cross-correlations between soft and hard X-ray bands. We also looked at the correlation functions in order to search for any characteristic timescales or periodicities that might be present in the data.

In Section 2 we discuss how we performed the data selection and reduction. In Section 3 we describe the approaches we used to compute auto-correlation functions, excess variances, hardness ratios and cross-correlation functions. We give the results of those analyses in Section 4. A discussion and our conclusions are in Section 5.

2 DATA SELECTION AND REDUCTION

The aim of this work is to search for and characterize the X-ray intra-day variability of Seyfert galaxies using *XMM-Newton*. For this purpose, we looked into archival data from this satellite for Seyfert galaxies and chose those sources which have the highest number of observations lasting longer than 30 ks, which are among the sources most often observed by *XMM-Newton*. Thanks to its excellent time resolution and ability to continuously point at specific X-ray sources for extended times, *XMM-Newton* is a superb X-ray observatory for time series analyses (Jansen et al. 2001). We have selected and analyzed time series data taken during 2000 to 2015 of three Seyfert galaxies: a total of 17 observations of NGC 4051, 7 of MCG-06–30–15 and 14 of NGC 4151 were taken when the sources were bright enough to provide sufficient count rates. We downloaded the data from the *XMM-Newton* Science archive. Our key selection criterion was that each observational duration exceeded 8 hours so we could probe and characterize the intra-day variability (IDV) from tens of minutes to a few hours. These observations use the European Photon Imaging Camera (EPIC) which has the ability to track the source continuously for many hours and its wide field of view is extremely beneficial for background subtraction. EPIC consists of three co-aligned CCD telescopes, MOS1, MOS2 and pn (Turner et al. 2001; Strüder et al. 2001). We only use the EPIC/pn (and not EPIC/MOS) because the former is least affected by pileup effects. We chose the energy range of $0.3-10.0$ keV for the light curve (LC) extraction because the data below 0.3 keV are significantly affected by pileup while those above 10 keV are seriously affected by background noise. All the observations considered here were taken in the small window (SW) mode.

We used *XMM-Newton* Science Analysis Software (SAS) version 15.0.0 for the data reduction. Event files were generated using the standard SAS routine *epchain*. The good time intervals (GTIs) were generated using *TABTIGEN* which contains the data devoid of proton flares. Then the cleaned event files were generated by combining the GTI and event list files and filtered using single and double event files (PATTERN $\leq$ 4) but excluding the events that are at the edge of the CCD (FLAG=0). To obtain the source event files, we have extracted an area of radius $30'' - 40''$, depending on the source location on the CCD. For background events, an area of radius $40'' - 50''$, located as far as away as possible from the source, is cho-

sen to avoid any of its contribution. Using *epiclccorr*, the background subtracted LCs were generated for the time bin of 100 s. We have checked for pileup effects for these observations using the SAS routine *epatplot* and found no significant pileup in any of the observations studied here.

Table 1 lists the observation log of *XXM-Newton* data for these three Seyfert galaxies. The first column provides the observation ID and the second column, the date when the observation was taken. The third column gives the revolution number of the satellite when the observation was taken. The fourth and fifth columns list the total good exposure time (GTI) and the mean count rate, μ, respectively.

3 LIGHT CURVE ANALYSIS TECHNIQUES

It is well established that many subclasses of AGNs, including Seyfert galaxies, show IDV in their X-ray LCs (e.g. Gaur et al. 2010; González-Martín & Vaughan 2012, Kalita et al. 2015; Gupta et al. 2016; Pandey et al. 2017, and references therein).

The *XMM-Newton* LCs of NGC 4051, MCG-06–30–15 and NGC 4151 for the observation IDs given in Table 1 are plotted in Figure 1. We made these LCs in the broad energy range 0.3–10 keV. By visual inspection, we can conclude that IDV is present in almost all the LCs and that during most of them significant flares were measured that rose and fell over the course of an hour or so. To obtain quantitative estimates of IDV timescales, if present, we have computed auto-correlation function (ACF) of the LCs to search for characteristic timescales in the IDV. Excess variance and fractional variance are used to calculate the IDV parameters. The X-ray variability parameters of observations are reported in Table 2. Brief descriptions of how we computed ACFs and excess variances are given in following subsections.

3.1 Auto-Correlation Function

The auto-correlation function (ACF) is the correlation between two values of the same variable at discretized times t_i and t_{i+k}. The ACF shows the relation between the past and future points of the data separated by a given time interval and so indicates the randomness or periodicity of the data. Given the measurements X_1, X_2,...,X_N, with mean $\bar{X}$, measured at times t_1, t_2,...,t_N, the ACF (r_k) at lag k for equally spaced observations is defined as

$$r_k = \frac{\Sigma_{i=1}^{N-k}(X_i - \bar{X})(X_{i+k} - \bar{X})}{\Sigma_{i=1}^{N}(X_i - \bar{X})^2}. \quad (1)$$

An ACF measures the relative strength of the signal and noise, as the presence of noise in the signal causes

the value of ACF to decrease with time. The presence of a peak at other than $\tau = 0$ signals the possible presence of periodicity of a QPO but the dips indicate the presence of characteristic timescales in the data (see section 3.2 of Pandey et al. 2017). If the binning is appropriate, the computed ACF will appear as the even function it should be, having the same value at the time lags t and $-t$ (Hufnagel & Bregman 1992; Hovatta et al. 2007).

In every case for these observations of NGC 4051, MCG-06–30–15 and NGC 4151, the ACFs gave putative timescales where minima are seen and where the monotonic declines away from the peak at $t = 0$ are followed by (usually modest) rises (Pandey et al. 2017); these dip timescales are listed as τ in Table 2 and range from 2.9 ks through 45.3 ks. In no case were there repetitive dips at nearly the same multiples of a lag time that might signal a QPO.

3.2 Excess Variance

Actual light curves are comprised of N flux measurements, x_i, along with their uncertainties, σ_i, for the ith time bin. The error arises mainly from measurement errors but as the typical X-ray source yields rather few photons per second, the error may also have a substantial Poisson contribution that adds to the total uncertainty. In order to obtain the intrinsic source variance, these errors needed to be subtracted (Nandra et al. 1997; Edelson et al. 2002). Let the mean square error, $\overline{\sigma_{\text{err}}^2}$, and sample variance, S^2, be defined respectively as

$$\overline{\sigma_{\text{err}}^2} = \frac{1}{N}\Sigma_{i=1}^{N}\sigma_i^2, \quad (2)$$

and

$$S^2 = \frac{1}{N-1}\Sigma_{i=1}^{N}(x_i - \bar{x})^2. \quad (3)$$

Then the excess variance is defined as

$$\sigma_{\text{XS}}^2 = S^2 - \overline{\sigma_{\text{err}}^2}. \quad (4)$$

The normalized excess variance is found by dividing the excess variance by the mean of the flux and the fractional root mean square (rms) variability is defined as its square root (Edelson et al. 1990; Rodríguez-Pascual et al. 1997)

$$F_{\text{var}} = \sqrt{\frac{S^2 - \overline{\sigma_{\text{err}}^2}}{\bar{x}^2}}. \quad (5)$$

This F_{var} gives the average variability amplitude with respect to the mean flux of the source and thus provides the rms variability in fractional terms. The uncertainty in the rms variability was calculated by Monte-Carlo simulations
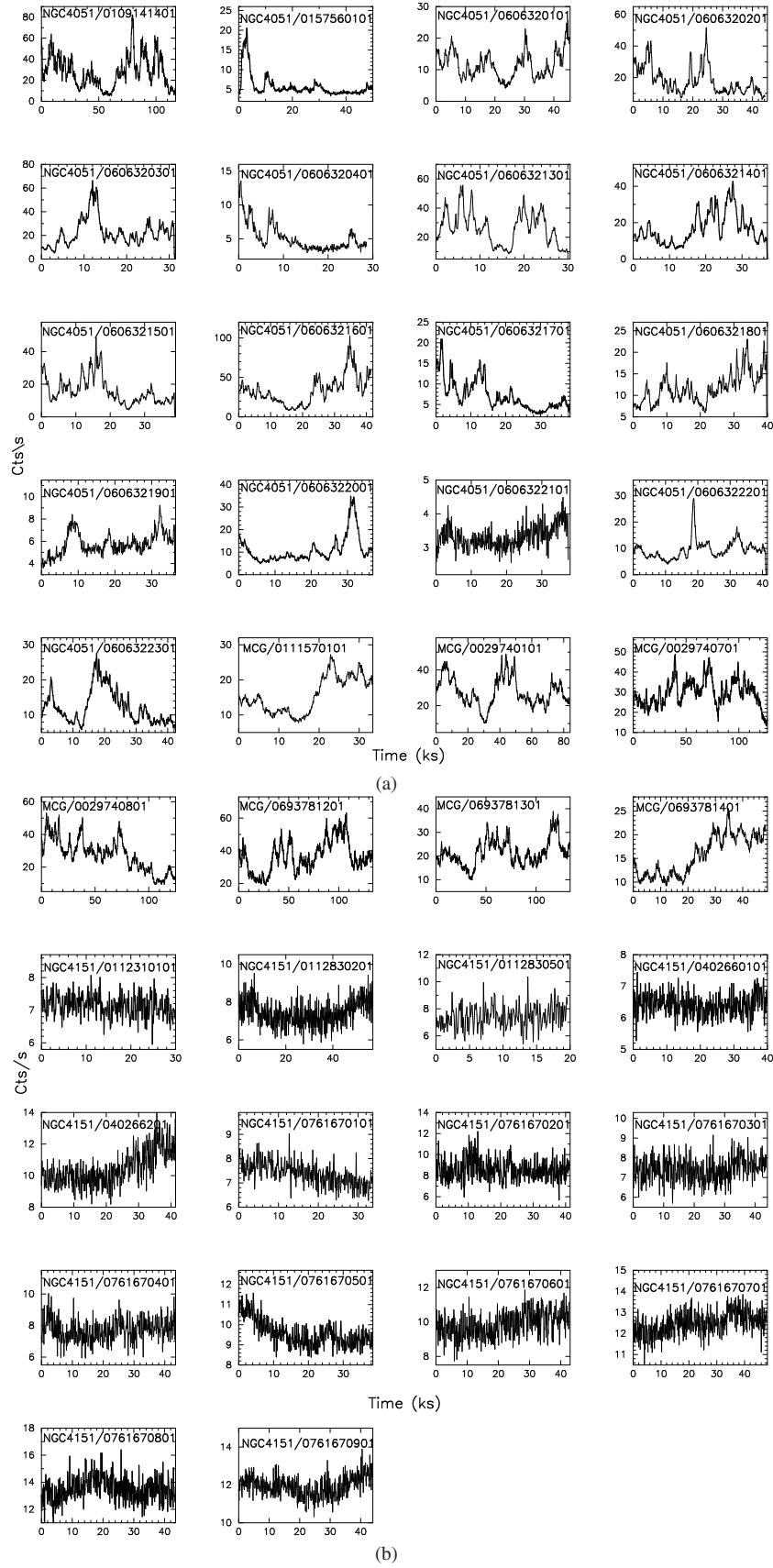
(a)

(b)

Fig. 1 (a) *XMM-Newton* light curves of the Seyfert galaxies NGC 4051 and MCG–06–30–15 (MCG) with the name and observation ID written in each panel. (b) As in Fig. 1(a) for MCG–06–30–15 (MCG) and NGC 4151.

Table 1 Log of *XMM-Newton* Observations of Three NLSy1s

Observation ID	Date of Observation	Revolution	GTI (s)	μ (ct s^{-1})
		NGC 4051		
0109141401	2001.05.16	263	116513	28.87±0.02
0157560101	2002.11.22	541	49710	5.74±0.12
0606320101	2009.05.03	1721	45236	11.49±0.02
0606320201	2009.05.05	1722	44346	18.02±0.02
0606320301	2009.05.09	1724	31268	22.27±0.03
0606320401	2009.05.11	1725	28750	5.10±0.02
0606321301	2009.05.15	1727	30138	25.98±0.04
0606321401	2009.05.17	1728	37992	16.42±0.03
0606321501	2009.05.19	1729	38789	16.02±0.02
0606321601	2009.05.21	1730	41453	33.49±0.03
0606321701	2009.05.27	1733	38297	7.20±0.02
0606321801	2009.05.29	1734	39886	11.61±0.02
0606321901	2009.06.02	1736	36419	5.75±0.01
0606322001	2009.06.04	1737	36893	10.97±0.02
0606322101	2009.06.08	1739	37621	3.32±0.01
0606322201	2009.06.10	1740	41084	9.49±0.01
0606322301	2009.06.16	1743	41978	12.23±0.02
		MCG-06–30–15		
0111570101	2000.07.11	108	41104	15.56±0.02
0029740101	2001.07.31	301	83335	27.71±0.02
0029740701	2001.08.02	302	126169	29.71±0.02
0029740801	2001.08.04	303	124369	27.62±0.02
0693781201	2013.01.29	2407	133710	36.43±0.02
0693781301	2013.01.31	2408	133640	21.49±0.02
0693781401	2013.02.02	2409	48459	27.71±0.02
		NGC 4151		
0112310101	2000.12.21	190	29963	7.13±0.02
0112830201	2000.12.22	190	56988	7.44±0.02
0112830501	2000.12.22	190	19700	7.41±0.06
0402660101	2006.05.16	1178	39932	6.42±0.02
0402660201	2006.11.29	1277	45611	10.43±0.04
0761670101	2015.11.12	2917	33574	7.39±0.02
0761670201	2015.11.14	2918	41116	8.57±0.04
0761670301	2015.11.16	2919	43654	7.41±0.03
0761670401	2015.11.30	2926	43443	7.73±0.03
0761670501	2015.11.20	2921	38345	9.56±0.02
0761670601	2015.11.22	2922	42612	9.86±0.03
0761670701	2015.12.16	2934	48023	12.48±0.02
0761670801	2015.12.18	2935	43435	13.49±0.04
0761670901	2015.12.22	2937	43942	11.93±0.02

described in Vaughan et al. (2003a) and can be given by (Jaffe et al. 2004)

$$(F_{\rm var})_{\rm err} = \sqrt{\left\{\sqrt{\frac{1}{2n}}\frac{\overline{\sigma_{\rm err}^2}}{\bar{x}^2 F_{\rm var}}\right\}^2 + \left\{\sqrt{\frac{\overline{\sigma_{\rm err}^2}}{n}}\frac{1}{\bar{x}}\right\}^2}. \quad (6)$$

Table 2 contains X-ray variability parameters for NGC 4051, MCG-06–30–15 and NGC 4151. The second and third columns represent excess variance and normalized excess variance, respectively, for the entire X-ray band. $F_{\rm var}$ values are given, along with their errors, in the fourth through sixth columns for the entire X-ray band considered, as well as for fluxes divided into soft (0.3–2.0 keV) and hard (2.0–10.0 keV) bands, respectively. The seventh

column of Table 2 gives the timescales indicated by the ACF for the overall LCs.

3.3 Soft and Hard X-ray Band Correlations

The spectrum of the source can give information about the physical processes responsible for its variation (Park et al. 2006 and references therein). Study of the spectra of each of these observations is beyond the scope of this paper, and in many cases the modest count rates would preclude us from producing decent spectra. However, there was a sufficiently high count rate in nearly every one of these *XMM-Newton* observations to allow us to examine the variations in the soft and hard bands separately. These individual LCs are shown in the left columns of Figure 3. It is clear from

Table 2 X-ray Variability Parameters for NLSy1s

Observation ID	σ^2_{XS} (total)	σ^2_{NXS} (total)	F_{var}(percent) Total (0.3–10 keV)	Soft (0.3–2 keV)	Hard (2–10 keV)	τ (ks)
NGC 4051						
0109141401	216.64	0.28	52.82±0.07	54.88±0.08	37.93±0.23	45.3
0157560101	8.11	0.24	49.37±0.21	49.23±0.22	57.92±0.58	4.7
0606320101	17.14	0.13	36.01±0.18	38.7±0.2	26.64±0.46	5.6
0606320201	74.53	0.23	47.92±0.14	50.04±0.15	35.44±0.42	9.3
0606320301	133.25	0.27	51.90±0.15	53.83±0.16	39.73±0.48	10.1
0606320401	4.06	0.16	39.48±0.36	40.97±0.39	37.66±0.86	3.5
0606321301	126.8	0.19	43.41±0.14	43.96±0.15	39.39±0.51	7.6
0606321401	69.39	0.26	50.89±0.16	52.72±0.17	39.41±0.52	13.7
0606321501	67.05	0.26	51.19±0.16	53.64±0.17	36.28±0.51	12.7
0606321601	315.81	0.28	53.06±0.10	54.66±0.11	40.59±0.34	19.1
0606321701	13.42	0.26	50.94±0.25	53.84±0.27	41.32±0.61	5.7
0606321801	12.18	0.09	30.11±0.20	30.41±0.21	29.08±0.5	2.9
0606321901	0.99	0.03	16.68±0.29	15.2±0.32	29.99±0.82	6.4
0606322001	35.32	0.03	54.25±0.21	56.39±0.22	46.36±0.59	7.6
0606322101	0.08	0.01	6.81±0.49	7.89±0.49	26.92±1.47	17.6
0606322201	12.73	0.14	37.64±0.21	39.31±0.23	34.51±0.58	8.3
0606322301	22.46	0.15	38.69±0.18	40.48±0.19	28.54±0.56	9.6
MCG-06–30–15						
0111570101	25.92	0.11	32.73±0.18	34.68±0.2	26.32±0.39	14.8
0029740101	63.54	0.08	28.76±0.08	29.78±0.09	25.59±0.2	19.4
0029740701	39.75	0.04	21.23±0.07	21.66±0.07	20.36±0.15	10.6
0029740801	96.32	0.13	35.53±0.07	36.13±0.08	33.86±0.16	44.0
0693781201	91.16	0.07	26.2±0.06	26.39±0.06	26.32±0.13	24.0
0693781301	28.87	0.06	24.99±0.08	25.01±0.08	26.04±0.17	34.6
0693781401	17.37	0.07	26.53±0.15	27.53±0.17	23.6±0.32	27.4
NGC 4151						
0112310101	-	-	–0.38±0.24	-	1.45±1.17	-
0112830201	0.14	0.002	4.97±0.4	3.82±0.98	8.04±0.5	30.8
0112830501	0.03	0.01	2.45±2.87	6.96±2.69	-	-
0402660101	0.01	0.0002	1.69±0.6	1.52±1.48	22.7±0.78	18.8
0402660201	0.62	0.005	7.55±0.4	-	9.74±0.47	22.4
0761670101	0.1	0.002	4.26±0.34	-	7.04±0.41	20.5
0761670201	0.23	0.003	5.56±0.82	–2.09±4.34	5.47±1.26	-
0761670301	0.02	0.001	2.28±0.98	2.52±1.958	4.67±0.92	-
0761670401	0.02	0.002	3.97±1.39	3.97±1.398	5.97±0.95	-
0761670501	0.28	0.003	5.57±0.24	-	8.8±0.28	21.4
0761670601	0.1	0.001	3.17±0.6	-	5.28±0.61	22.1
0761670701	0.1	0.001	2.43±0.24	1.82±0.88	3.41±0.26	9.8
0761670801	0.15	0.001	2.92±0.48	-	4.56±0.48	13.3
0761670901	0.11	0.001	2.76±0.24	-	4.14±0.27	17.5

those figures that usually the fractional variations in the soft band exceed those in the hard, though there are exceptions. This impression is quantified through values of F_{var} computed and shown in the fourth through sixth columns of Table 2.

The cross correlation function (CCF) is a measure of the degree to which the data points of different time series are correlated at a particular time delay. The CCF calculates how the points of a particular data set (X_1, X_2,...,X_i,...,X_N) are related to the points of another data set (Y_1, Y_2,...,Y_{i+k},...,Y_N), occurring with a time delay k as,

$$r_k = \frac{\Sigma_{i=1}^{N-k}(X_i - \bar{X})(Y_{i+k} - \bar{Y})}{\sqrt{\Sigma_{i=1}^{N}(X_i - \bar{X})^2}\sqrt{\Sigma_{i=1}^{N}(Y_i - \bar{Y})^2}}. \quad (7)$$

Here $\bar{X}$ and $\bar{Y}$ are the means of the X and Y data, respectively. The CCFs between the soft and hard X-ray bands are given in the middle columns in Figure 3. A peak at a non-zero time indicates that one of the bands consistently led the other as they varied. When the two data sets are same, then the CCF is simply the ACF discussed in Section 3.1.

As is frequently done, we employ the hardness ratio (HR) as a simple proxy for the spectrum, defining it as

$$HR = \frac{H - S}{H + S}, \quad (8)$$

where here H refers to the hard X-ray flux (2.0–10 keV) and S is its soft counterpart (0.3–2.0 keV). These HR plots as functions of time are shown in the right columns of Figure 3.

4 RESULTS

4.1 NGC 4051

NGC 4051 is an NLSy1 galaxy first observed in X-rays by the *Einstein Observatory* (Marshall et al. 1983). Peterson et al. (2000) claimed that the frequently seen rapid X-ray variability is not observed in optical observations even when correlated on the timescales of many weeks and longer. Lamer et al. (2003) reported the X-ray variability observed by *RXTE* observations during 1996–1999 when the flux of NGC 4051 varied by a factor of about 100.

A tight correlation between extreme ultraviolet emission from *EUVE* and continuum X-ray emission from *RXTE* was found by Cagnoni et al. (1999) who concluded that its SMBH mass is $2.0 - 8.0 \times 10^7\ M_\odot$. *Chandra* observations of NGC 4051 in 2000 (Collinge et al. 2001) indicated the absence of significant soft X-ray emission.

Breedt et al. (2010) presented a cross-correlation study using X-ray and optical light curves spanning more than 12 years which confirmed that the amplitude of optical variability is much less than that of X-rays. Light curves in the optical band were found to be well correlated at around 1 day, which is consistent with the time taken by light to cross the optical emitting region and suggests that optical variations are driven by X-ray reprocessing. Alston et al. (2013) used *XMM-Newton* and *Swift* data to analyze light curves of NGC 4051 and found no significant correlation between UV and X-ray emission, though the UV was variable on both short and long time-scales.

Out of the 17 *XMM-Newton* observations of NGC 4051, one was taken in 2001, one in 2002 and the rest in 2009. We note that the mean count rates for the full band show the source was in a high flux state during the 2001 observation while it was in low flux state in the 2002 observation. We also note that these mean count rates for the full band varied by a factor of 10 over the course of 3 weeks in 2009, and that they frequently change by a factor of 2 or more between subsequent observations that are only 2 or 4 days apart. In every case for these observations of NGC 4051, the ACFs gave putative timescales where minima are seen and where the monotonic declines away from the peak at $t = 0$ are followed by rises (Pandey et al. 2017); these dip timescales are listed as τ in Table 2 and range from 2.9 ks through 45.3 ks. The mean value of these timescales 11.16 ± 9.91 ks. In no case were there repetitive dips at nearly the same multiples of a lag time that might signal a QPO.

We see that for every observation but one, the CCFs peak at zero lag and have correlation coefficients exceeding 0.8 at that time. This implies that the hard and soft fluxes typically vary synchronously and their photons arise from essentially the same physical process and are apparently co-spatial. The exception to this strong correlation is seen in the CCF computed for Obs. ID 0606322101, but those data are very noisy, having the lowest count rates of all 17 observations, so the nominal lag of ~ 17 ks indicated by its CCF is not at all trustworthy. Using *Suzaku* data, Miller et al. (2010) did find a time lag between its hard and soft bands of ~ 970 s while McHardy et al. (2004) noted the possibility of one of ~ 3000 s in the *XMM-Newton* data for 2001.

We note from the separate LCs for the soft and hard X-rays in the left columns of those figures that the soft flux tends to vary proportionately more than does the hard flux. That translates into the HRs usually getting softer (more negative) during flares and harder during quiescent periods, as is clear from a comparison of the LCs and the HRs for each source. There are, however, exceptions to that trend. One such case is for the single observation made during 2002 (Obs. ID 0157560101) when the HR remained essentially flat, despite the presence of one major flare and a couple of minor ones. The other three exceptions, however, correspond to the faintest states and so may be dominated by noise.

4.2 MCG-06–30–15

MCG-06–30–15 is an NLSy1 galaxy situated at a distance of 37 Mpc ($z = 0.008$). It was first observed as a point X-ray source in June 1976 with the *SAS-3* X-ray satellite (Pineda et al. 1979). Vaughan et al. (2003b) reported a strong correlation between rms variability amplitude and flux which was previously seen only in X-ray binaries. Arévalo et al. (2006) analyzed the 300 ks 2001 *XMM-Newton* observation to study correlation between 0.2–10.0 X-ray and 300–400 nm UV bands and found them to be significant.

Of the seven *XMM-Newton* observations of MCG-06–30–15, one was taken in 2000, three in 2001 and the other three in 2013. We note that these mean count rates for the full band show the source was in moderate and high flux states during the 2001 and 2013 observations while it was in a somewhat lower flux state during the 2000 observation. We also note that these mean count rates for the full band are almost the same in 2001 and 2013. In every case for these observations of MCG-06–30–15, the ACFs gave putative timescales where minima are seen and where the monotonic declines away from the peak at $t = 0$ are followed by rises (e.g. Pandey et al. 2017); these dip timescales are listed as τ in Table 2 and range from 10.6 ks
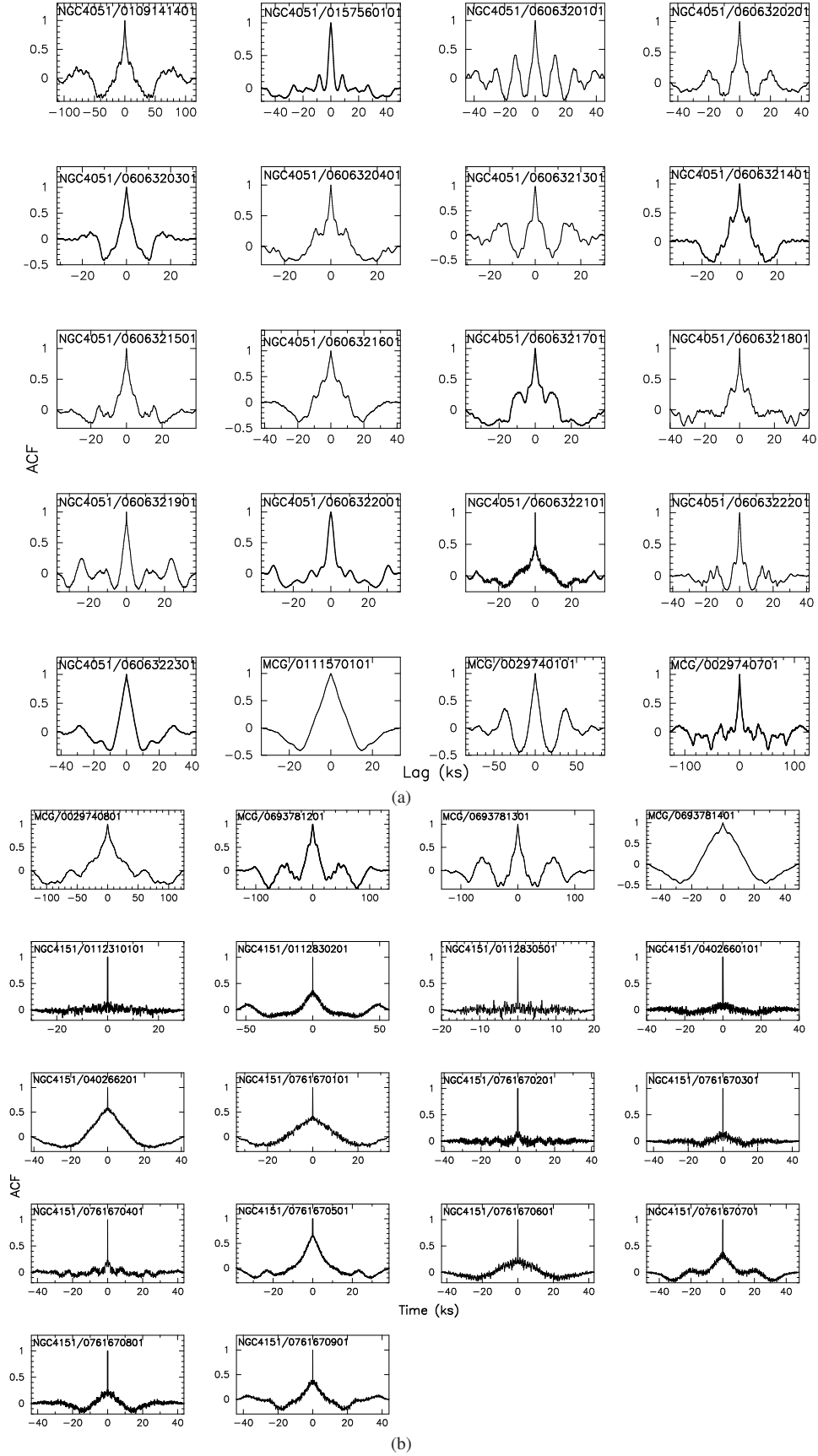
Fig. 2 (a) Auto-correlation functions (ACFs) for NGC 4051 and MCG–06–30–15 (MCG), with object name and observation number labeling each panel. (b) As in Fig. 2(a) for MCG–06–30–15 (MCG) and NGC 4151.
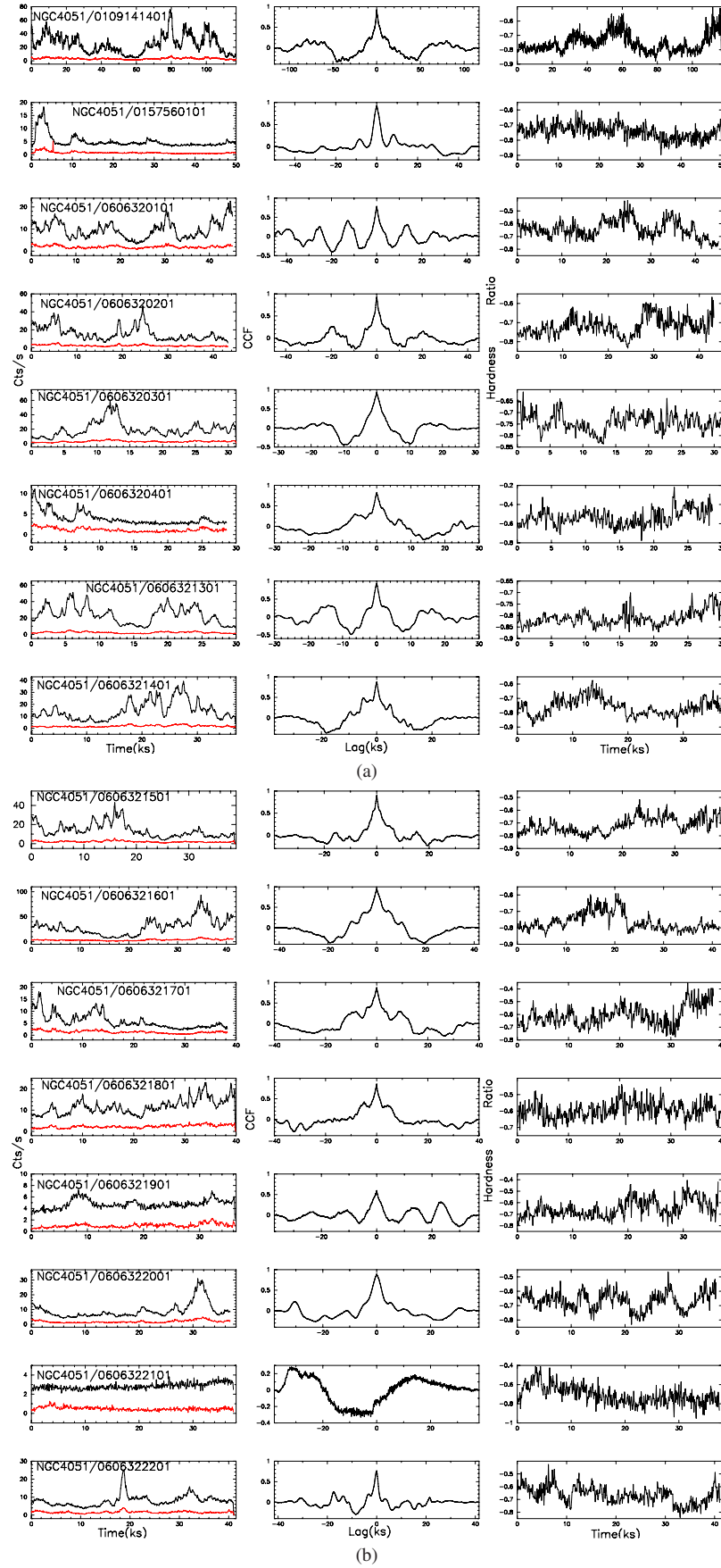
Fig. 3 (a) Soft (0.3–2 keV, in *black*) and hard (2–10.0 keV, in *red*) light curves (*left panels*). Cross correlation functions (CCFs) between those bands (*middle panels*) and hardness ratios (*right panels*) are plotted for the observations of NGC 4051 labeled in the LCs. (b) For NGC 4051.
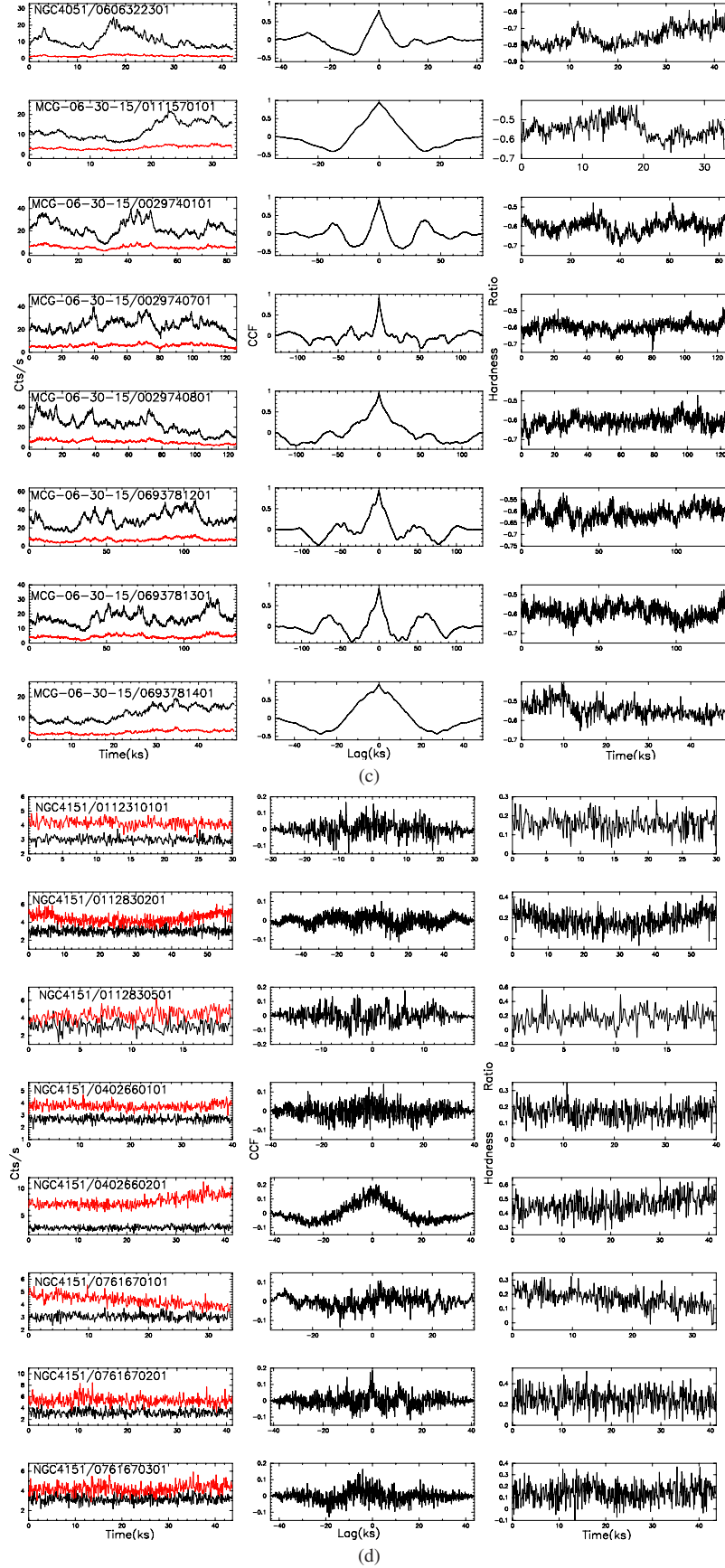
Fig. 3 —*Continued.* (c) For NGC 4051 and MCG-06–30–15. (d) For NGC 4151.
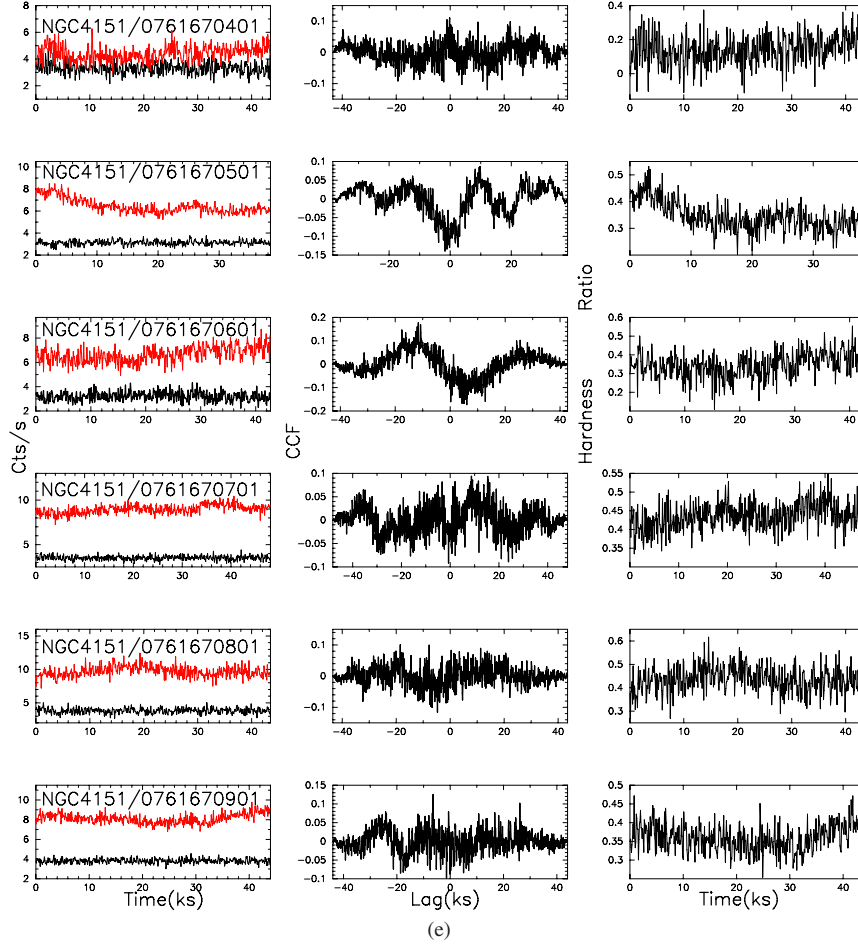
Fig. 3 —*Continued.* (e) For NGC 4151.

through 44.0 ks. In no case were there repetitive dips at nearly the same multiples of a lag time that might signal a QPO.

The separate LCs for the soft and hard X-rays in the left columns of those figures show that the soft flux tends to vary proportionately more than does the hard flux. Thus, the HRs usually are softer during flares and harder during quiescent periods.

4.3 NGC 4151

NGC 4151 is a close-by ($z = 0.003319$) and well studied Seyfert 1.5 galaxy possessing a clear bright stellar nucleus. It was observed by the *Uhuru* satellite during 1970–1971 when it was detected and reported as an X-ray source for the first time.

Oknyanskij et al. (2006) studied correlations between the infrared and optical variability and found that the time delay between optical and NIR variation changes with time and is correlated with the state of nuclear processes in the source. Another correlation between the optical lumi-

nosity of this AGN and the time lag between UV/optical and NIR light curves was interpreted as thermal dust reverberation (Minezaki et al. 2006). Onken et al. (2014) found the SMBH mass of this source to be $3.76 \pm 1.15 \times 10^7 \, M_\odot$. Keck et al. (2015) presented the X-ray timing and spectral analysis of simultaneous 150 ks of *NuSTAR* and *SUZAKU* observations taken during November 2012 and found strong evidence of relativistic reflection from an inner accretion disk. Landt et al. (2015) studied coronal line variability in this source using simultaneous optical, IR and X-ray observations. Recently, Edelson et al. (2017) analyzed the *Swift* observation of the source taken in 2016 and reported UV/optical bands to be significantly correlated with X-rays. The variability within those UV/optical bands also is correlated.

XMM-Newton provided a total of 14 LCs of NGC 4151 of which three were taken in 2000, two in 2006 and the remaining nine in 2015. The mean count rates for the full band show the source was in moderate and low flux states during most of the observations. We also note that these mean count rates for the full band did not even
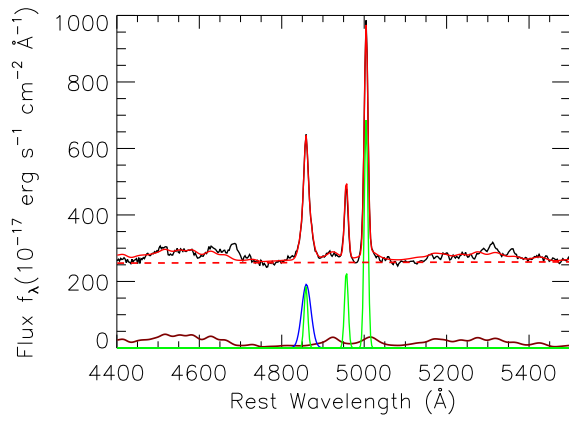
Fig. 4 Fit to the spectrum of NGC 4051. The continuum is modelled with a power law (*red dashed line*) and Fe II emission (*brown line*). The Hβ line (4861 Å) is fitted with one gaussian for the broad component (*blue*) and one gaussian (*green*) for the narrow component.

Fig. 5 Fit to the spectrum of MCG-06–30–15, as in Fig. 4.

Fig. 6 Fit to the spectrum of NGC 4151. The continuum is again modelled with a power law (*red dashed line*). The Paβ line (12820 Å) is fitted with one gaussian for the broad component (*blue*) and a gaussian (*green*) for the narrow component.

vary by a factor of 2 over the entire set of observations. In every case for these observations of NGC 4151, the ACFs gave putative timescales where minima are seen and where the monotonic declines away from the peak at $t = 0$ are followed by rises; these dip timescales are listed as τ in Table 2 and range from 9.8 ks through 30.8 ks. Like the other sources, in no case were there repetitive dips at nearly the same multiples of a lag time that might signal a QPO.

The CCFs for NGC 4151 are much weaker than for the other two sources, rarely exceeding 0.15. These thus usually show no preference for any particular lag, or at most for a mild one at 0 lag. This result can be attributed primarily to the weaker variations exhibited by this source that make computations of lags difficult and secondarily to the somewhat lower overall count rates. The spectra of NGC 4151 are substantially harder than those of the other two sources, having positive instead of negative HR values. They show a mild tendency to be harder when brighter, though there are no strong flares seen during any of the 14 observations.

5 BLACK HOLE MASS ESTIMATION

In order to study the difference of BH masses estimated in a uniform way between these NLSy1 and Seyfert 1.5 galaxies, we analysed the optical or near-infrared (NIR) spectrum for these three sources. The local continuum of the line we focussed on (Hβ for NGC 4051 and MCG-06–30–15, and Paβ for NGC 4151) is modelled with single power law (plus iron emission, if necessary). We used Gaussian functions to fit the emission line after subtracting the continuum (Guo & Gu 2014, Shen et al. 2011).
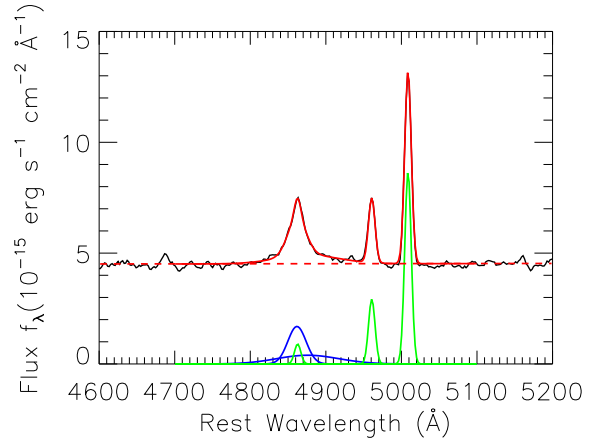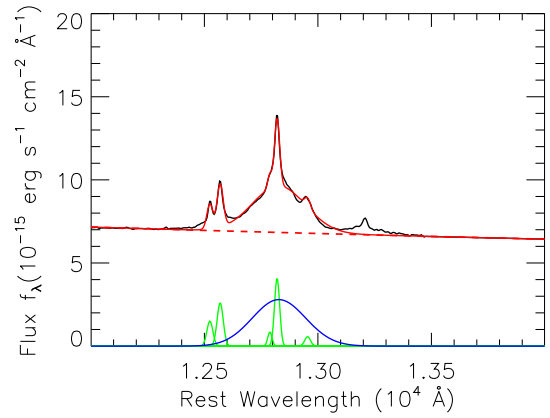
The nuclear optical spectroscopy of NGC 4051 is taken from the NED[1] database, where the data were taken at the 2.3 m Bok Telescope (Moustakas & Kennicutt 2006). For this source (Fig. 4), Hβ can be well modelled by one broad component with full width at half maximum (FWHM) at 1625.4 km s^{-1} and a narrow component. The black hole (BH) mass is calculated by using this FWHM and the luminosity of Hβ line ($\log (L_{H\beta}) = 38.81$ erg s^{-1}; see Vestergaard & Peterson 2006). This gives us $M_{BH} = 0.12(\pm 0.11) \times 10^6 \, M_\odot$. The result is found to be consistent, within the errors, with the value found using reverberation mapping in Denney et al. (2010).

The optical spectral data of MCG-06–30–15 were obtained from an observation in 2008 in the public archive of the Lick Observatory 3 m Shane telescope (Bentz et al. 2009). As Figure 5 demonstrates, the Hβ line is characterized by two broad components with FWHM at

---

[1] *http://ned.ipac.caltech.edu/*

1993 km s^{-1} and one narrow component. The BH mass is calculated in the same way as for NGC 4051 ($\log(L_{\mathrm{H}\beta}) = 40.09$) and found to be $M_{\mathrm{BH}} = 1.15(\pm0.8) \times 10^6\ M_\odot$. This black hole mass estimation is in reasonable agreement with that found in Bentz et al. (2016).

The near-infrared spectrum data of the spectra of NGC 4151 was also download from the NED database. It was observed by the NASA 3 m Infrared Telescope Facility (IRTF) on 2002 April 23 and was discussed by Riffel et al. (2006). For NGC 4151 (Fig. 6), we use one Gaussian to fit the broad component of the Paβ line with FWHM of 6445.2 km s^{-1} and one Gaussian for the narrow component. The SMBH mass is estimated by using the broad FWHM and luminosity of Paβ ($\log(L_{\mathrm{Pa}\beta}) = 40.27$ erg s^{-1}; see Kim et al. 2010), which gives the estimate for the mass of the black hole to be $M_{\mathrm{BH}} = 8.2(\pm0.5\ \mathrm{dex}) \times 10^7\ M_\odot$. Our value is somewhat higher than that found in Bentz et al. 2006; $4.57 \times 10^7\ M_\odot$) but is consistent considering the uncertainties.

6 DISCUSSION AND CONCLUSIONS

We have examined the LCs for timescales using ACFs and have also considered the cross-correlations between the hard and soft bands and hardness ratios. NGC 4051 was quite active during essentially all of these observations, with individual LCs often showing flares that produce a change of a factor of 5 or more in count rates. Over the entire set of observations the mean X-ray fluxes (0.3–10 keV) of the individual observations varied by just about a factor of 10. The more limited observations of MCG-06–30–15 showed a great deal of activity during individual flares, with fluxes usually varying by factors of 2–3, but with relative stability overall, with mean counts changing by only about a factor of 2. While there were also many measurements made of NGC 4151, this source was not doing much of interest, typically changing by less than 20% during an individual LC, though the overall flux range was roughly a factor of 2.

In the case of NGC 4151, the ACF values always dropped down to much lower values very soon after zero lags as compared to other sources; this implies that the strength of the signal relative to the noise is low. For the other two objects the ACF values almost always fall more gradually, indicating that the strength of signal is high and the noise does not dominate. Hence the variability timescales obtained for NGC 4051 and MCG-6-30-15 are more reliable as the noise contribution is low.

Our cross-correlations between the hard (2–10 keV) and soft (0.3–2 keV) bands show that they are very well correlated on sub-day timescales for NGC 4051 and MCG-6-30-15. Using the hardness ratio to get a feel for the spectral variability, we find that these two sources typically soften during flares.

The independent estimates of the black hole mass we have made are in reasonable accord with earlier measurements. They reinforce the hypothesis that NLSy1 galaxies have relatively low mass black holes and hence, high Eddington ratios.

References

Alston, W. N., Vaughan, S., & Uttley, P. 2013, MNRAS, 429, 75

Arévalo, P., Papadakis, I., Kuhlbrodt, B., & Brinkmann, W. 2006, in ASPC, 360, AGN Variability from X-Rays to Radio Waves, eds. C. M. Gaskell, I. M. McHardy, B. M. Peterson, & S. G. Sergeev, 127

Bentz, M. C., Denney, K. D., Cackett, E. M., et al. 2006, ApJ, 651, 775

Bentz, M. C., Walsh, J. L., Barth, A. J., et al. 2009, ApJ, 705, 199

Bentz, M. C., Cackett, E. M., Crenshaw, D. M., et al. 2016, ApJ, 830, 136

Boller, T., Brandt, W. N., & Fink, H. 1996, A&A, 305, 53

Breedt, E., McHardy, I. M., Arévalo, P., et al. 2010, MNRAS, 403, 605

Cagnoni, I., Fruscione, A., McHardy, I. M., & Papadakis, I. E. 1999, Mem. Soc. Astron. Italiana, 70, 29

Collinge, M. J., Brandt, W. N., Kaspi, S., et al. 2001, ApJ, 557, 2

Denney, K. D., Peterson, B. M., Pogge, R. W., et al. 2010, ApJ, 721, 715

Edelson, R. A., Krolik, J. H., & Pike, G. F. 1990, ApJ, 359, 86

Edelson, R., & Nandra, K. 1999, ApJ, 514, 682

Edelson, R., Turner, T. J., Pounds, K., et al. 2002, ApJ, 568, 610

Edelson, R., Gelbord, J., Cackett, E., et al. 2017, ApJ, 840, 41

Espaillat, C., Bregman, J., Hughes, P., & Lloyd-Davies, E. 2008, ApJ, 679, 182

Gaur, H., Gupta, A. C., Lachowicz, P., & Wiita, P. J. 2010, ApJ, 718, 279

Gierliński, M., Middleton, M., Ward, M., & Done, C. 2008, Nature, 455, 369

González-Martín, O., & Vaughan, S. 2012, A&A, 544, A80

Goodrich, R. W. 1989, ApJ, 342, 224

Guo, H., & Gu, M. 2014, ApJ, 792, 33

Gupta, A. C., Kalita, N., Gaur, H., & Duorah, K. 2016, MNRAS, 462, 1508

Hovatta, T., Tornikoski, M., Lainela, M., et al. 2007, A&A, 469, 899

Hufnagel, B. R., & Bregman, J. N. 1992, ApJ, 386, 473

Ishibashi, W., & Courvoisier, T. J.-L. 2009, A&A, 504, 61

Jaffe, W., Meisenheimer, K., Röttgering, H. J. A., et al. 2004, Nature, 429, 47

Jansen, F., Lumb, D., Altieri, B., et al. 2001, A&A, 365, L1

Kalita, N., Gupta, A. C., Wiita, P. J., Bhagwan, J., & Duorah, K. 2015, MNRAS, 451, 1356

Keck, M. L., Brenneman, L. W., Ballantyne, D. R., et al. 2015, ApJ, 806, 149

Kim, D., Im, M., & Kim, M. 2010, ApJ, 724, 386

Komossa, S., & Xu, D. 2007, ApJ, 667, L33

Lachowicz, P., Gupta, A. C., Gaur, H., & Wiita, P. J. 2009, A&A, 506, L17

Lamer, G., McHardy, I. M., Uttley, P., & Jahoda, K. 2003, MNRAS, 338, 323

Landt, H., Ward, M. J., Steenbrugge, K. C., & Ferland, G. J. 2015, MNRAS, 449, 3795

Markowitz, A., Edelson, R., Vaughan, S., et al. 2003, ApJ, 593, 96

Marshall, F. E., Holt, S. S., Mushotzky, R. F., & Becker, R. H. 1983, ApJ, 269, L31

McHardy, I. M., Gunn, K. F., Uttley, P., & Goad, M. R. 2005, MNRAS, 359, 1469

McHardy, I. M., Papadakis, I. E., Uttley, P., Mason, K. O., & Page, M. J. 2004, Nuclear Physics B Proceedings Supplements, 132, 122

Miller, L., Turner, T. J., Reeves, J. N., et al. 2010, MNRAS, 403, 196

Minezaki, T., Yoshii, Y., Aoki, T., et al. 2006, in Astronomical Society of the Pacific Conference Series, 360, AGN Variability from X-Rays to Radio Waves, eds. C. M. Gaskell, I. M. McHardy, B. M. Peterson, & S. G. Sergeev, 79

Moustakas, J., & Kennicutt, Jr., R. C. 2006, ApJS, 164, 81

Nandra, K., George, I. M., Mushotzky, R. F., Turner, T. J., & Yaqoob, T. 1997, ApJ, 476, 70

Oknyanskij, V. L., Lyuty, V. M., Taranova, O. G., & Shenavrin, V. I. 2006, in ASPC 360, AGN Variability from X-Rays to Radio Waves, eds. C. M. Gaskell, I. M. McHardy, B. M. Peterson, & S. G. Sergeev, 75

Onken, C. A., Valluri, M., Brown, J. S., et al. 2014, ApJ, 791, 37

Pan, H.-W., Yuan, W., Yao, S., et al. 2016, ApJ, 819, L19

Pandey, A., Gupta, A. C., & Wiita, P. J. 2017, ApJ, 841, 123

Papadakis, I. E. 2004, MNRAS, 348, 207

Park, T., Kashyap, V. L., Siemiginowska, A., et al. 2006, ApJ, 652, 610

Peterson, B. M., McHardy, I. M., Wilkes, B. J., et al. 2000, ApJ, 542, 161

Pineda, F., Delvaille, J., Grindlay, J., Huchra, J., & Schnopper, H. 1979, in BAAS, 11, Bulletin of the American Astronomical Society, 427

Riffel, R., Rodríguez-Ardila, A., & Pastoriza, M. G. 2006, A&A, 457, 61

Rodríguez-Pascual, P. M., Alloin, D., Clavel, J., et al. 1997, ApJS, 110, 9

Shen, Y., Richards, G. T., Strauss, M. A., et al. 2011, ApJS, 194, 45

Strüder, L., Briel, U., Dennerl, K., et al. 2001, A&A, 365, L18

Turner, M. J. L., Abbey, A., Arnaud, M., et al. 2001, A&A, 365, L27

Vaughan, S., Edelson, R., Warwick, R. S., & Uttley, P. 2003, MNRAS, 345, 1271

Vaughan, S., Fabian, A. C., & Nandra, K. 2003, MNRAS, 339, 1237

Vaughan, S., Uttley, P., Pounds, K. A., Nandra, K., & Strohmayer, T. E. 2011, MNRAS, 413, 2489

Véron-Cetty, M.-P., Véron, P., & Gonçalves, A. C. 2001, A&A, 372, 730

Vestergaard, M., & Peterson, B. M. 2006, ApJ, 641, 689

Wagner, S. J., & Witzel, A. 1995, ARA&A, 33, 163

Zhou, X.-L., Yuan, W., Pan, H.-W., & Liu, Z. 2015, ApJ, 798, L5